AGU PUBLICATIONS

Geophysical Research Letters

RESEARCH LETTER
10.1002/2017GL075989

Special Section:
New understanding of the solar eclipse effects on geospace: The 21 August 2017 Solar Eclipse

Ionospheric Total Electron Content Response to the Great American Solar Eclipse of 21 August 2017

Iurii Cherniak[1] and Irina Zakharenkova[2]

[1]COSMIC Program Office, University Corporation for Atmospheric Research, Boulder, CO, USA, [2]West Department of IZMIRAN, Kaliningrad, Russia

Abstract Using a comprehensive database of ~4,000 ground-based Global Navigation Satellite Systems stations, we investigate the ionosphere's response to the 21 August 2017 solar eclipse. The high-resolution, two-dimensional maps of the ionospheric total electron content (TEC) were constructed using combined GPS and GLONASS measurements. Solar eclipse resulted in a continent-size TEC decrease with stronger effects up to 50% over the U.S. eastern coast. Along the totality path within an area of 75% obscuration TEC decreased by ~30–40%. We reveal a latitudinal dependence of the TEC response with equatorward expansion of TEC depletion. Recovery signature in the form of large-scale TEC enhancement up to 20–30% occurred in posteclipse period. Swarm and DMSP satellites encountered the eclipse-induced plasma density depletion and posteclipse increase at 450 km height and above. These effects were associated with downward plasma fluxes from topside ionosphere/plasmasphere and thermospheric changes.

Key Points:
- Solar eclipse resulted in a continent-size TEC decrease with stronger effects up to 50% over the U.S. eastern coast
- Recovery signature in the form of large-scale TEC enhancement up to 30% occurred in posteclipse period over North America
- Swarm and DMSP satellites observations indicates eclipse-induced density depletion and posteclipse increase at 450 km height and above

Supporting Information:
- Supporting Information S1
- Movie S1

Correspondence to:
I. Cherniak,
iurii@ucar.edu

Citation:
Cherniak, I., & Zakharenkova, I. (2018). Ionospheric total electron content response to the great American solar eclipse of 21 August 2017. *Geophysical Research Letters*, *45*, 1199–1208. https://doi.org/10.1002/2017GL075989

Received 13 OCT 2017
Accepted 29 DEC 2017
Accepted article online 8 JAN 2018
Published online 5 FEB 2018

©2018. American Geophysical Union. All Rights Reserved.

1. Introduction

The long-lasting passage of a total solar eclipse over a region with dense instrumental network is an extremely rare event and represents a great opportunity to study in detail eclipse-induced ionospheric effects. In past decades, the ionospheric response to solar eclipses has been studied by different observation techniques such as scarcely distributed ionosondes (Chen et al., 2013; Evans, 1965) and incoherent scatter radars (Cherniak & Lysenko, 2013; MacPherson et al., 2000; Salah et al., 1986) and, recently, by using ground-based GNSS (Global Navigation Satellite Systems) measurements. During a solar eclipse, reduce in solar EUV flux results in thermosphere-ionosphere cooling, electron density decrease at $E/F_1/F_2$ regions and decrease in the total electron content (TEC), integrated up to 20,000 km. For total eclipse that occurred at midlatitudes, TEC depletion can reach 30–40% with time delay of 5–20 min (Ding et al., 2010; Jakowski et al., 2008), for high latitudes TEC decreased by 10–30% (Afraimovich et al., 1998; Hoque et al., 2016; Momani et al., 2010). TEC response to total eclipses at equatorial latitudes is complicated by equatorial anomaly and can reach more than 30–40% (Tsai & Liu, 1999).

On 21 August 2017 a total solar eclipse traveled across the continental United States from the Pacific to the Atlantic Oceans in ~95 min. For the first time, a total solar eclipse traverses over an unprecedented dense observational network—more than 4,000 GNSS stations. No other country or region in the world has such a numerous GNSS network. GNSS-based experimental technique with accurate, continuous, and high-resolution measurements enables absolutely new perspective on eclipse-induced dramatic ionosphere's changes with unprecedented details and becomes possible for the 21 August 2017 solar eclipse.

Recently, Huba and Drob (2017) reported first simulation prediction of the 21 August 2017 eclipse impact on the ionosphere/plasmasphere system. Here we present a comprehensive overview of the ionospheric density response to eclipse as deduced from dense ground-based GNSS observations.

2. Data and Methods Used

We used an extensive database consisting of ~4,000 ground-based GNSS stations in North America gathered from several GNSS networks. These stations collect signals from ~8 to 12 different GPS satellites per epoch. Apart from GPS signals ~2,600 stations receive simultaneously signals transmitted by another GNSS—Russian Global Navigation Satellite System (GLONASS). We considerably increase a number of available

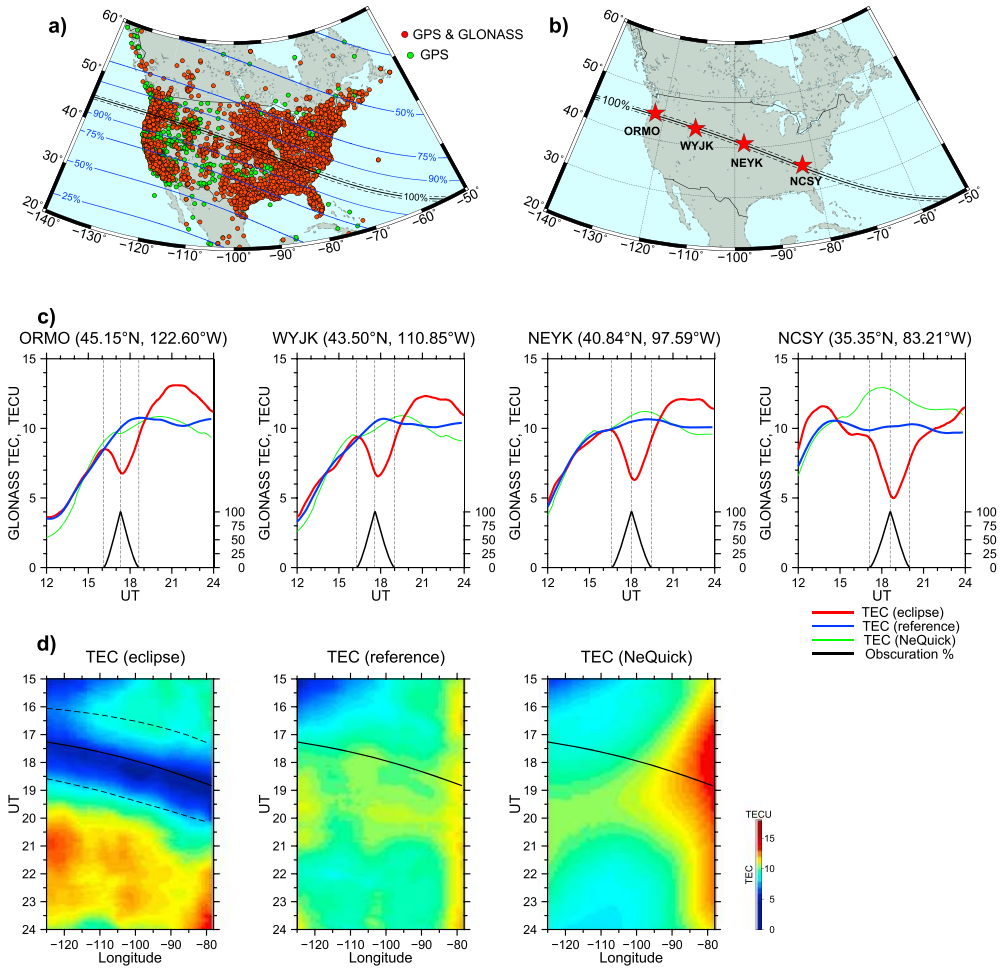

Figure 1. (a) Geographical location of multi-GNSS (red dots) and GPS (green dots) stations with superimposed solar eclipse totality path (black lines) and 90%, 75%, 50%, and 25% solar obscuration (blue) lines. (b) Location of GNSS stations within totality path and (c) GLONASS TEC variations as a function of time (UT) for eclipse day (red curve), reference day (blue curve), and NeQuick TEC (green curve); vertical dotted lines depict eclipse start, maximum, and end time; right vertical axis shows percentage for obscuration (black curve). (d) TEC variation along totality path as a function of UT and longitude for eclipse day, reference day, and NeQuick simulations. Solid line shows totality path; dashed lines show begin and end of partial eclipse.

observations with processing GLONASS signals by factor of 1.5–2 comparing to GPS only. Figure 1a shows distribution of ground-based GNSS stations illustrating substation contribution of GLONASS. The ionospheric TEC is a number of electrons integrated along line-of-sight receiver satellite. We calculate absolute vertical TEC values from raw GNSS measurements using original technique (Zakharenkova et al., 2016). We select elevation cutoff angle as 35° to avoid multipath effects and minimize numbers of TEC observations from low-elevated satellites. We construct TEC maps over North America at 2 min time intervals by averaging and binning of all GNSS-derived TEC values into cells of 0.5° × 0.5° in geographic latitude/longitude. No interpolation was applied; cells with no data were marked as blank ones. This approach allows to study in detail the rapid ionospheric density changes and irregular structures (Cherniak & Zakharenkova, 2016).

3. Results

The 21 August 2017 solar eclipse began at 15:46 UT over Pacific and ended at 21:04 UT over Atlantic Oceans. The total eclipse started at 16:49 UT and ended at 20:02 UT, totality (umbral) shadow traversed the United States from 17:14 UT till 18:48 UT, approximately 95 min. Figure 1a shows a map of GNSS stations with the superimposed solar eclipse totality path and obscuration lines. The dense network has an ideal location to track the eclipse with obscuration from 50% to 100%. We present results of ionospheric TEC behavior for

the eclipse day of 21 August 2017 relative to reference level, calculated as a mean of both preeclipse and posteclipse days of 20 and 22 August 2017, respectively. Geomagnetic conditions for this period were rather quiet. Our processing technique allows retrieving precise TEC values for all visible satellite passes over a GNSS station, which further used for diurnal TEC variations and two-dimensional TEC maps.

We consider four GNSS stations located within the totality path (Figure 1b). Figure 1c presents diurnal TEC variations retrieved from GLONASS measurements for eclipse and reference days. TEC values are presented in TEC units (1 TECU = 10^{16} el/m^2). To illustrate a climatological TEC behavior, we plot TEC simulated by the NeQuick-2 model for geophysical conditions of the eclipse day. NeQuick-2 is an empirical ionospheric model able to calculate TEC up to GNSS altitudes (Nava et al., 2008). The climatological TEC variation is very close to reference TEC behavior over three midlatitude stations and reveals differences for lower latitude station NCSY.

On the eclipse day TEC values changed from the normal climatological diurnal behavior. For all stations diurnal TEC variations demonstrate clear TEC drop during the eclipse time. TEC began to decrease gradually after the first touch of penumbral shadow. TEC decrease had minimum with ~15–20 min lag after eclipse maximum. Then TEC gradually increased, reaching reference values in ~1 h after eclipse end.

Figure 1d presents absolute TEC values, calculated with 0.5° step along the totality path as function of UT and longitude for eclipse and reference days and NeQuick-2 results. NeQuick simulations reproduce well the normal diurnal TEC behavior over the United States and can be used as additional control reference. Reference TEC values, calculated from preeclipse and posteclipse days, are in a very close agreement with NeQuick-2 results for all longitudes except of larger model values near 80°W. For eclipse day, we find that (1) eclipse started in different LT conditions, (2) TEC depression occurred during eclipse time at all longitudes, and (3) noticeable posteclipse TEC enhancement occurred at all longitudes. Observed TEC enhancement is much larger than TEC values of reference day and NeQuick model, which is contrary to the model predictions of eclipse effects. Huba and Drob (2017) reported that after eclipse passes overhead the TEC increases but it does not reach the value of control simulation by the run end (24 UT). Our results demonstrate that ground-based TEC recovered to preeclipse values over all locations along the totality path (Figure 1d).

To reveal signatures of the eclipse-induced ionosphere's modification with high spatiotemporal resolution, we analyze differential TEC (dTEC) maps. The high-resolution dTEC maps were constructed on a cell-by-cell basis with respect to TEC values of reference days. Figure 2 presents maps of absolute and percentage dTEC values for specific instants of time. Full set of dTEC maps with 2 min time interval during 15–24 UT on 21 August 2017 is available in Movie S1 (supporting information).

Figure 2a shows preeclipse conditions at 15:30 UT on 21 August 2017. Over continental United States we observe slight dTEC variations within ±1 TECU. Figure 2b illustrates conditions for 17:14 UT when total eclipse reached U.S. West Coast, while the penumbral shadow covered most of the United States. Here total eclipse occurred in the morning, when daytime ionosphere was still forming. Within solar obscuration zone of 75% TEC depletion was −3–4 TECU (~30%). Figures 2c–2f demonstrate further evolution of TEC reaction to eclipse passage over United States till 19 UT, when totality zone left the continent. From these figures and Movie S1 we note that (1) TEC depletion covered the whole continent, (2) magnitude of TEC depletion and size of the affected zone rose with eclipse passage from west to east, (3) from central to the eastern United States the TEC decreased by −5–6 TECU (~40–50%), (4) TEC started to decrease in response to 10–15% solar obscuration, and (5) most dramatic TEC changes occurred within 75% obscuration zone.

Another distinguish feature is a posteclipse TEC enhancement. During recovery phase TEC reached preeclipse levels at all locations and continued to further increase (Figure 2g). The pronounced TEC enhancement appeared at 21 UT from higher latitudes over the western United States. Later, the large TEC enhancement zone expanded over the whole continent (Figure 2h). TEC increased up to ~2–3 TECU (~20–30%). Movie S1 shows TEC increase development in more detail. For all longitudes from west to east, TEC increase appeared firstly at high latitudes and then moved equatorward. Such behavior most likely relates with downward plasma flux from the plasmasphere caused by plasma temperature decrease during the eclipse.

Figure S1 (supporting information) illustrates the same sequence of maps with absolute and percentage dTEC values as Figure 2, but with respect to NeQuick TEC simulations for the eclipse day. The model-data dTEC values are in a good qualitative and quantitative agreement with results of reference day (Figure 2);

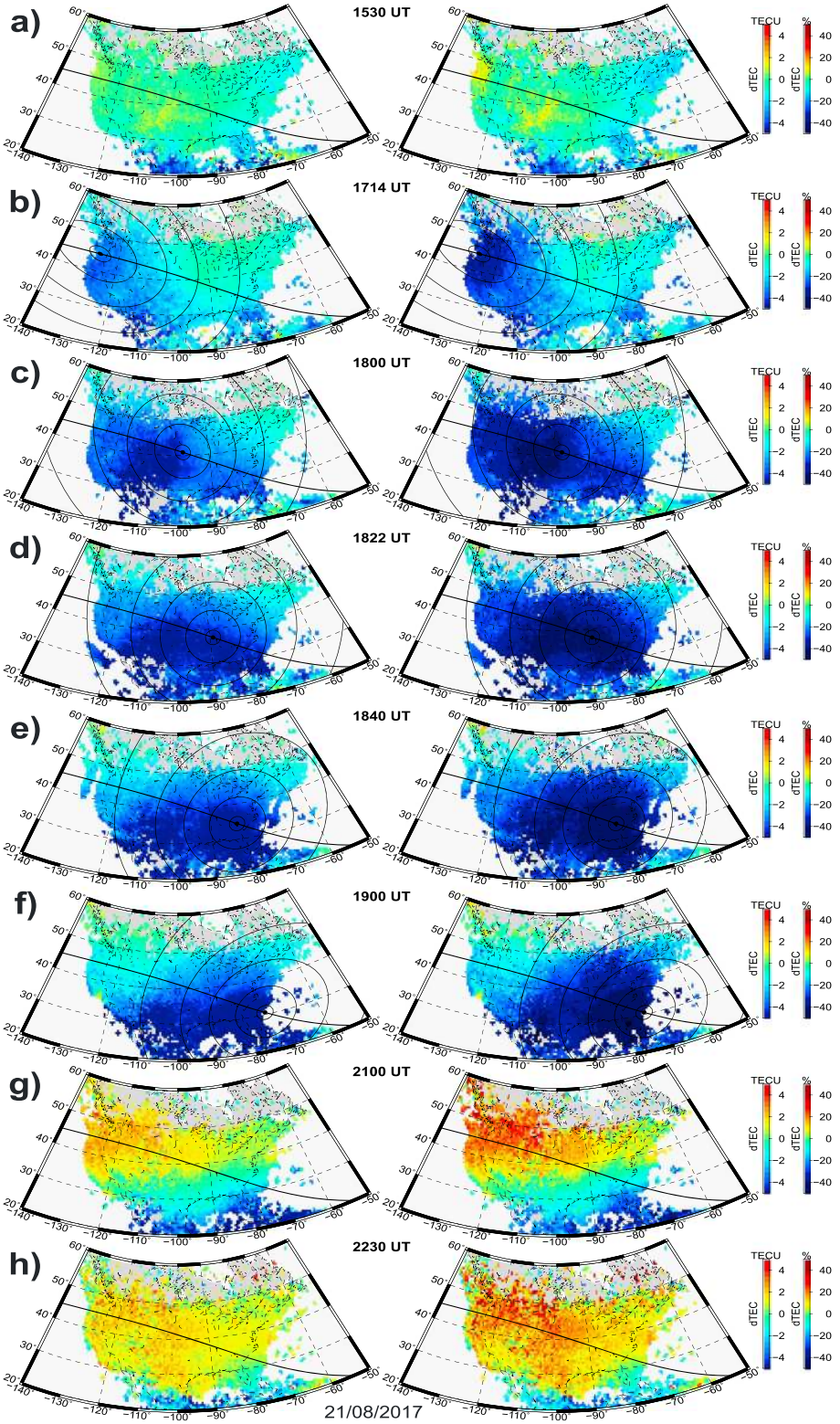

Figure 2. Two-dimensional maps of absolute (left column) and percentage (right column) dTEC values for (a–h) specific moments of time on 21 August 2017. Thick black line shows the eclipse path; thin lines depict 95%, 75%, 50%, 25%, and 0% solar obscuration zone. Full set of two-dimensional maps with 2 min interval is available in Movie S1.

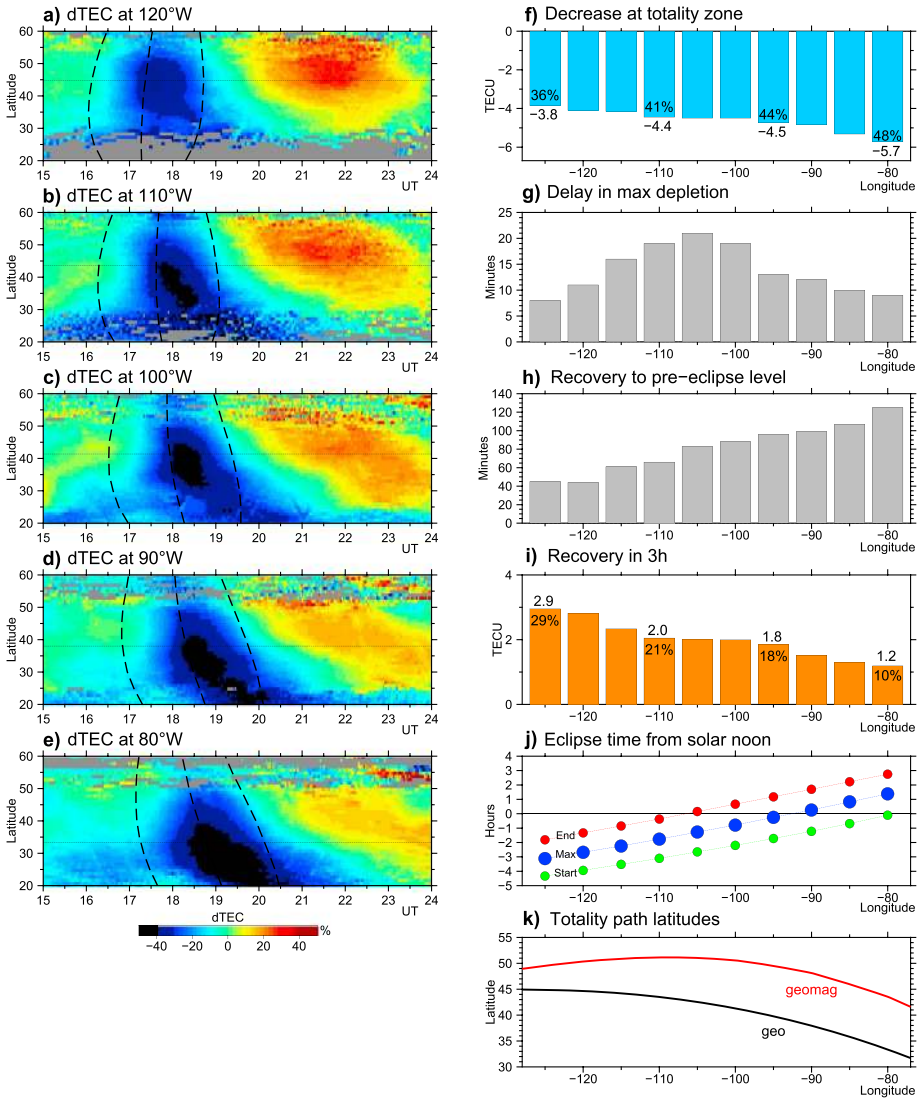

Figure 3. (a–e) Percentage dTEC values as a function of latitude and time, evaluated along different longitudes in North America; dashed lines depict the eclipse start, maximum, and end time; horizontal line shows the total eclipse latitude. (f) Extreme TEC decrease in absolute and percentage values within the totality zone for different longitudes. (g) Time lag of extreme TEC decrease from maximum eclipse time. (h) Time of TEC recovery to preeclipse level. (i) TEC increase in 3 h after the eclipse end. (j) Difference of eclipse time from solar noon. (k) Geographical (black) and geomagnetical (red curve) latitudes of totality path.

they reproduce eclipse-induced TEC depletion and posteclipse TEC enhancement. Figure S2 (supporting information) presents absolute TEC maps for eclipse and reference days and NeQuick for more evident illustration that reference TEC results agreed well with climatological TEC specification for eclipse day conditions. Figures S2g and S2h demonstrate significant differences of TEC distribution pattern during posteclipse hours with respect to both reference day and climatological estimates.

To analyze longitudinal effects we compare evolution of eclipse-induced TEC changes with time. Figures 3a–3e present meridional slices of percentage dTEC values at selected longitudes. The eclipse-induced TEC depression was clearly observed over all longitudes with pronounced differences. The weaker TEC decrease was over the West Coast (120°W); here TEC dropped by ~35–37%. For other longitudes TEC decrease exceeded 40%. The maximal TEC depletion zone stretches equatorward from the totality latitude by 10°–15°. In time, this zone appeared mainly from the maximum eclipse time till ~60% obscuration for totality latitude and till ~20% obscuration at lower latitudes. The largest eclipse effects in TEC appeared over eastern United States (90°W–80°W), reaching 45–52%. We found the TEC recovery to preeclipse level with following noticeable TEC enhancement during posteclipse phase over all longitudes. Meridional dTEC slices clearly

recognize TEC increase starting after the eclipse end; it appeared at higher latitudes near 50°–60°N, northward from eclipse path, and farther at lower latitudes. Zone of maximal TEC enhancement (~20–30%) appeared in ~2–3 h after eclipse end and located mainly northward from eclipse path.

Figure 3f demonstrates TEC depression magnitude within the totality zone (±1° from the central line) at different longitudes. TEC depression was deepening from west to east in absolute values, from −3.8 to −5.7 TECU, and percentage from 36% to 48%. Maximal TEC decrease located southward of eclipse path. Figure 3g shows time lag of maximal TEC decrease from maximum eclipse time. Time lag of 15–20 min was observed over 100°–110°W, minimal values of 8–10 min were found over eastern and western coasts. Figure 3h shows how fast the TEC recovered to preeclipse values. Fastest recovery (less 1 h) was registered over western longitudes with much longer recovery (~2 h) over eastern coast. Figure 3i presents dTEC change within the totality zone 3 h after eclipse end. TEC exceeded the preeclipse and reference levels at all longitudes (Figure 3i). With an opposite trend, the most pronounced TEC enhancement of ~3 TECU (~30%) was registered over western United States, while the smallest one of 1.2 TECU (10%) was observed over eastern coast.

The substantial longitudinal effect in dTEC can be explained by different circumstances of eclipse occurrence in LT. Figure 3j shows discrepancies of eclipse time (start, maximum, and end) from solar noon time. At the west, eclipse began and ended in the morning time ionosphere, while at the east eclipse began and ended during afternoon, where plasma loss rate and transport processes already dominate over production rate. TEC depletion magnitude over different longitudes related to background ionospheric conditions before eclipse appearance. We observe a latitudinal effect with much smaller TEC response to the north from totality path and further TEC enhancements developed at higher latitudes. It can be explained by larger downward flux at higher latitudes, which can mitigate the eclipse-induced electron density depression at higher latitudes. The eclipse-induced local reduction in electron temperature results in pressure reduction and downward plasma flux from topside ionosphere/plasmasphere. The larger downward plasma flux is expected to be at higher latitudes with the larger dip angle. This dip angle effect was simulated and discussed by Le et al. (2009).

The totality path moved in latitude from 44.9°N over the West Coast to 33.7°N over East Coast, resulted in eclipse movement to lower latitudes with higher background electron density. However, totality path was practically along the same geomagnetic latitude (~49°–50°magnetic latitude) for 125°W–95°W longitudes. As ionospheric plasma is transported along geomagnetic field line and eclipse-driven ionospheric disturbances affected flux tubes with similar volumes, we observe posteclipse TEC enhancement of similar magnitude northward from the totality path due to downward field-aligned plasma motion. The smallest time lag of TEC depression peak (~10 min) occurred over western area can be explained by smaller TEC depression during local morning, while small time lag over eastern zone corresponds to local afternoon and lower geomagnetic latitudes. Thus, all revealed longitudinal and latitudinal differences in TEC response between east/west regions can be explained by combination of different LT of eclipse occurrence (Figure 3j) and geomagnetic latitude of totality (Figure 3k).

Additionally, we analyze ionospheric data provided by Swarm, which is only one mission flying at altitudes close to the ionospheric F_2 peak. Fortunately, tandem of Swarm A and C satellites separated by ~1.4° in longitude passed over North America during eclipse time. The Swarm A (SWA) passes at ~445 km altitude were in ascending nodes at ~11.8 LT. We consider in situ electron density (Ne) measurements by Langmuir probe and calculate up-looking TEC from onboard GPS receiver (Zakharenkova & Cherniak, 2015). SWA up-looking TEC represents plasma density contribution above 445 km toward topside ionosphere/plasmashere. Figures 4a and 4b show Ne and TEC observations along SWA passes comparing with preeclipse day. We observe a close similarity in behavior of in situ Ne and up-looking TEC.

The first SWA pass (Figure 4a) was at ~101°W longitude; SWA intersected the shadow zone in ~40 min after the total eclipse passage. The satellite encountered clear density depletion within ±15° from the totality path. The observed Ne decrease close to the totality zone was up to 3×10^4 el/cm^3, roughly 38% relative to the control day. Prominent decrease in up-looking TEC was up to 1.5–2 TECU, which means that topside ionosphere above 445 km contributes approximately by 30% to the ground-based TEC decrease of ~5–6 TECU, while 70% of electron density reduce comes from the altitudinal range of 100–450 km. Second SWA pass (Figure 4a) appeared over western coast at ~20:10 UT, ~1.5 h after eclipse end. That time corresponds to

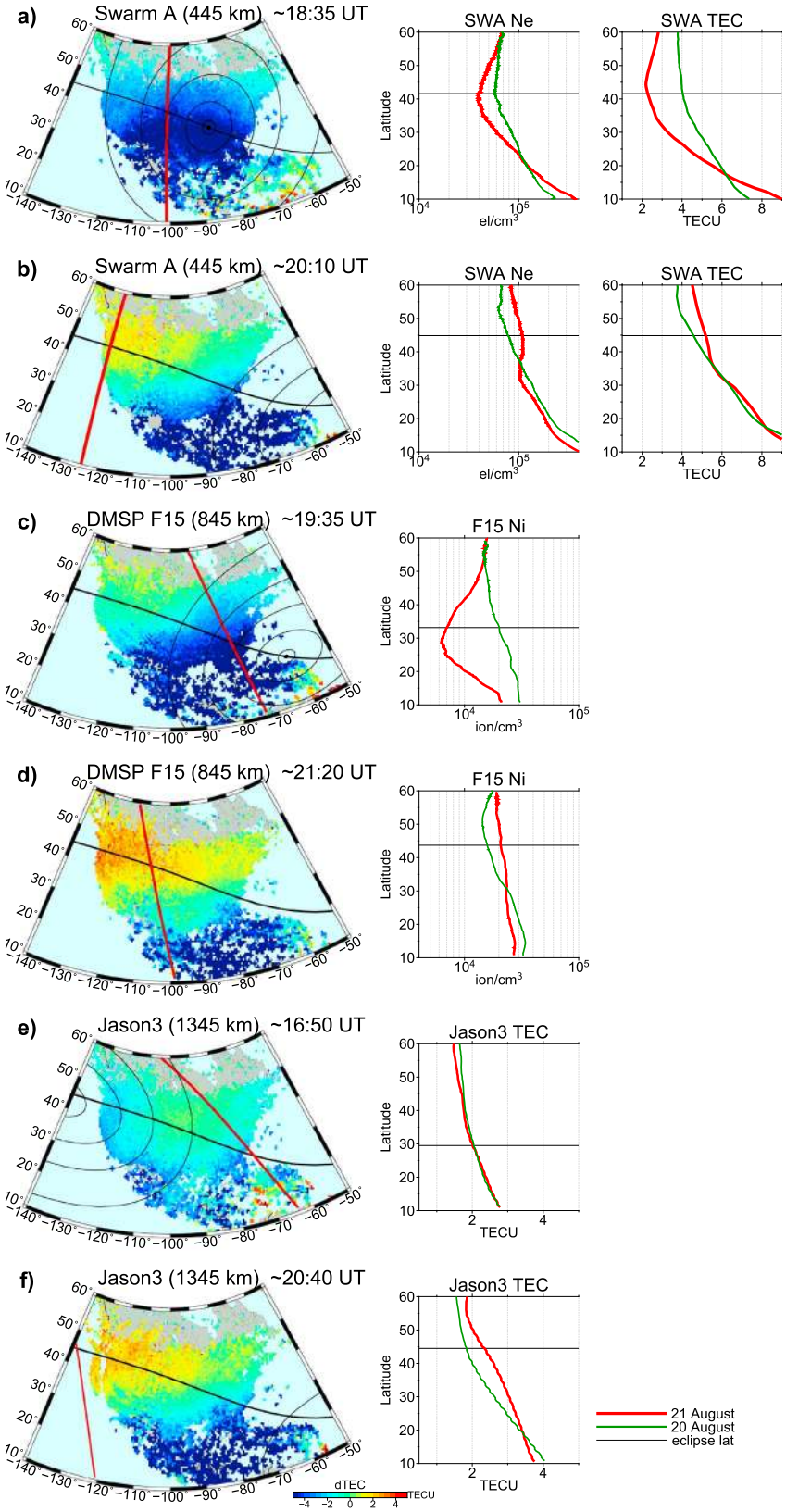

Figure 4. (left column) Two-dimensional dTEC maps with superimposed satellite passes (red lines) during eclipse day, the eclipse path, and solar obscuration (black lines); (right column) in situ plasma density and up-looking TEC along passes of (a, b) Swarm A, (c, d) DMSP F15, and (e, f) Jason-3 satellites, as compared with pre-eclipse day (green curve).

recovery posteclipse phase when TEC started to increase (Figures 2g and 2h and Movie S1). Both Ne and up-looking TEC demonstrate an increase within 40°–60°N latitude range. The up-looking TEC increase up to ~1 TECU contributes roughly 75–80% to the ground TEC enhancement, which confirms the plasmasphere contributed to the recovery TEC enhancement. The identical signature of Ne/TEC values was found with Swarm C satellite. Further, DMSP F15 satellite (Figure 4c) crossed the zone with maximal TEC depletion, revealed over the western United States (cf. Figure 3e), and encountered ion density depletion at altitudes of ~845 km at ~19:35 UT. Next F15 pass (Figure 4d) appeared in the posteclipse phase and demonstrated larger density over region with TEC enhancement with respect to reference track. The up-looking TEC above ~1335 km derived from Jason-3 GPS measurements revealed no differences between eclipse and preeclipse days for 16:50 UT (before eclipse, Figure 4e) but confirmed the posteclipse TEC enhancement at plasmaspheric altitudes (Figure 4f).

4. Summary

For the first time, a total solar eclipse was observable during ~95 min by an unprecedented number of GNSS stations (~4,000). Use of GLONASS system allows to increase a number of observational data by factor 1.5–2 comparing with GPS only. We presented the detailed overview of ionospheric TEC response to the total eclipse using a very large amount of simultaneous observations. The 21 August 2017 total eclipse provides a great opportunity to investigate how midlatitude ionosphere responses to an eclipse with regard to longitudinal, latitudinal, local time, and obscuration effects. We found that the eclipse resulted in a continent-size decrease in TEC. TEC decreased by ~30–40% along the totality path within an area of 75% obscuration. TEC decrease had ~8–20 min lag after maximal eclipse time depending on LT and location.

The largest response in TEC by ~40–50% was observed over the eastern United States. That was a result of several contributing factors: (1) TEC response was more intense at lower geomagnetic latitudes where eclipse path moved and (2) eclipse overpassed this region in later LT (noon-afternoon). Much weaker TEC response was observed over the western coast at the background circumstances of the morning-rise ionosphere.

We found a clear effect of nonuniform latitudinal dependence of eclipse-induced TEC response. The much smaller TEC response occurred to the north from totality path, while a major part of TEC depletion stretches by 10°–15° equatorward from the totality latitude. The integrated plasma density, descried by vertical TEC, results from balance between ionization sources, loss, and transport processes. The eclipse-induced local reduction in electron temperature will result in pressure reduction and downward plasma flux from the topside ionosphere/plasmasphere. From the other side, ion recombination when solar ionization source switched off is more effective at lower latitudes taking into account higher neutral mass density.

We found rather good agreement with the SAMI3 model simulations that predicted TEC decrease up to −5 TECU (35%) for the greatest eclipse time at 18:36 UT (Huba & Drob, 2017). Our results reveal that over eastern United States the TEC decreased up to −5–6 TECU (~40–50%). In contrast with SAMI3 model predictions, we observe that TEC recovered to preeclipse values and exceeded reference level (observations and NeQuick model) over whole United States. The fastest recovery was registered over western longitudes where eclipse occurred in the morning and recovery coincided with prenoon/noon time.

The prominent feature was the posteclipse TEC enhancement, appeared in ~1 h at latitudes above 50°N and followed after eclipse shadow. The daytime TEC enhancement was up to ~2–3 TECU (~20–30%) and observed during several hours. Analysis of the ionosonde data on Idaho and Boulder stations (not shown) reveals long-lasting (20-23UT) increase of F_2 peak height by ~20–30 km and N_mF_2 increase by 25–30%, consistent with collocated TEC observations. Swarm and DMSP satellites observations revealed eclipse-induced plasma density depletion and posteclipse increase at ~450 km and ~835 km height. TEC enhancement above ~1,335 km derived from Jason-3 GPS measurements also confirmed the posteclipse TEC enhancement at plasmaspheric altitudes. Four satellites by different instruments have revealed posteclipse enhancement at different altitudes in the topside.

The posteclipse increase of ionospheric density was first reported by Evans (1965) and explained by plasma flux similar to the evening midlatitude f_oF_2 increase. So effects of TEC enhancement can be partially explained in terms of downward plasma flux. A simplest scenario of such processes includes (1) upward plasma flows from the ionosphere during sunlight time in the presence of active ionization and heating processes in

bottomside ionosphere and (2) downward flux when plasma production switches off in the bottom ionosphere. So after the maximal eclipse plasma can flow downward from topside ionosphere/plasmasphere (similar to downward fluxes after sunset), whereas the recovered source of ionization induces rapid plasma production in the bottomside ionosphere after eclipse end. The preliminary results of the Millstone Hill Incoherent scatter radar Regional Vector Eclipse campaign (not shown here, but available in Madrigal database) demonstrates increase of ion velocity vertical component in downward direction up to 100 m/s after 19:30 UT, end of eclipse main phase over radar.

As downward plasma motion is more inertial process than bottomside ionization, these two plasma sources coexist at the same time. So, both bottomside and topside regions with raised plasma population lead to a joint enhancement signature in TEC. During posteclipse time, Figures S2g and S2h demonstrate TEC recovery to reference level due to ionization recovery at lower latitudes and noticeable TEC enhancement at much higher latitudes (above totality).

The question is what process can sustain long-lasting TEC enhancement after electron temperature recovery (~2 h after eclipse, J. Huba, private communication, 2017). Korenkov et al. (2003) modeled such posteclipse f_oF_2 increase of ~10% with GSM-TIP Model for August 1999 eclipse and they associated such effects with perturbations in the thermospheric parameters (temperature and neutral density). In particular, $[N_2]$ density was remaining decreased for ~12 h afterward. As a result of rapid [O] restore and decreased $[N_2]$ densities, the $[ON_2]$ ratio increased and caused increased f_oF_2/N_mF_2 after eclipse. Müller-Wodarg et al. (1998) in the CTIP modeling study also explained posteclipse N_mF_2 enhancement by increased $[ON_2]$ ratio after Tn minimum in posteclipse time. These simulations indicated [O] increase due to eclipse-induced cooling and downwelling and $[N_2]$ drop due to downwelling and atmosphere expansion after temperature increase during recovery.

So obtained results for August 2017 solar eclipse demonstrate that ionospheric plasma disturbances and thermospheric changes initiated by eclipse can be superposed with dynamic processes associated with plasma fluxes from topside ionosphere/plasmasphere, which were not directly impacted by eclipse.

Only first principal models give an opportunity to establish numerical experiment of ionospheric and thermospheric response to eclipse not affected by day-to-day variability. Future simulating efforts are required to estimate timescales and impact magnitude of dynamic processes on the thermosphere/ionosphere/plasmasphere coupled system.

Acknowledgments
We acknowledge use of GNSS data provided by UNAVCO (ftp://data-out.unavco.org), IGS (ftp://cddis.gsfc.nasa.gov), CORS (ftp://geodesy.noaa.gov), SmartNet (support.smartnetna.com), FPRN (www.myfloridagps.com), Natural Resources Canada (webapp.geod.nrcan.gc.ca), and CHAIN (ftp://chain.physics.unb.ca/gps/). We thank ESA for Swarm data (http://earth.esa.int/swarm), NOAA/NCEI for DMSP data (https://satdat.ngdc.noaa.gov/dmsp/data/), and Jason data (www.class.ngdc.noaa.gov). We thank J. Huba and A. Richmond for helpful discussions. I. C. was supported by National Science Foundation CAS AGS-1033112 and I. Z. by Russian Foundation for Basic Research grant 16-05-01077.

References

Afraimovich, E. L., Palamartchouk, K. S., Perevalova, N. P., Chemukhov, V. V., Lukhnev, A. V., & Zalutsky, V. T. (1998). Ionospheric effects of the solar eclipse of March 9, 1997, as deduced from GPS data. *Geophysical Research Letters*, *25*, 465–468. https://doi.org/10.1029/98GL00186

Chen, G., Qi, H., Ning, B., Zhao, Z., Yao, M., Deng, Z., … Wu, C. (2013). Nighttime ionospheric enhancements induced by the occurrence of an evening solar eclipse. *Journal of Geophysical Research: Space Physics*, *118*, 6588–6596. https://doi.org/10.1002/jgra.50551

Cherniak, I., & Zakharenkova, I. (2016). First observations of super plasma bubbles in Europe. *Geophysical Research Letters*, *43*, 11,137–11,145. https://doi.org/10.1002/2016GL071421

Cherniak, I. V., & Lysenko, V. N. (2013). Measurements of the ionosphere plasma electron density variation by the Kharkov Incoherent Scatter Radar. *Acta Geophysica*, *61*(5), 1289–1303. https://doi.org/10.2478/s11600-013-0118-0

Ding, F., Wan, W., Ning, B., Liu, L., Le, H., Xu, G., … Yang, M. (2010). GPS TEC response to the 22 July 2009 total solar eclipse in East Asia. *Journal of Geophysical Research*, *115*, A07308. https://doi.org/10.1029/2009JA015113

Evans, J. V. (1965). On the behavior of f_oF_2 during solar eclipses. *Journal of Geophysical Research*, *70*, 733–738. https://doi.org/10.1029/JZ070i003p00733

Hoque, M. M., Wenzel, D., Jakowski, N., Gerzen, T., Berdermann, J., Wilken, V., … Minkwitz, D. (2016). Ionospheric response over Europe during the solar eclipse of March 20, 2015. *Journal of Space Weather and Space Climate*, *6*. https://doi.org/10.1051/swsc/2016032

Huba, J. D., & Drob, D. (2017). SAMI3 prediction of the impact of the 21 August 2017 total solar eclipse on the ionosphere/plasmasphere system. *Geophysical Research Letters*, *44*, 5928–5935. https://doi.org/10.1002/2017GL073549

Jakowski, N., Stankov, S., Wilken, V., Borries, C., Altadill, D., Chum, J., … Cander, L. R. (2008). Ionospheric behaviour over Europe during the solar eclipse of 3 October 2005. *Journal of Atmospheric and Solar: Terrestrial Physics*, *70*(6), 836–853. https://doi.org/10.1016/j.jastp.2007.02.016

Korenkov, Y. N., Klimenko, V. V., Baran, L. W., Shagimuratov, I. I., & Bessarab, F. S. (2003). Model calculations of TEC over Europe during 11 August 1999 solar eclipse. *Advances in Space Research*, *31*(4), 983–988. https://doi.org/10.1016/S0273-1177(02)00815-3

Le, H., Liu, L., Yue, X., Wan, W., & Ning, B. (2009). Latitudinal dependence of the ionospheric response to solar eclipses. *Journal of Geophysical Research*, *114*, A07308. https://doi.org/10.1029/2009JA014072

MacPherson, B., Gonzfilez, S. A., Sulzer, M. P., Bailey, G. J., Djuth, F., Rodriguez, P., … Rodriguez, P. (2000). Measurements of the topside ionosphere over Arecibo during the total solar eclipse of February 26, 1998. *Journal of Geophysical Research*, *105*, 23,055–23,067. https://doi.org/10.1029/2000JA000145

Momani, M. A., Yatim, B., & Mohd Ali, M. A. (2010). Ionospheric and geomagnetic response to the total solar eclipse on 1 August 2008 over Northern Hemisphere. *Journal of Geophysical Research*, *115*, A08321. https://doi.org/10.1029/2009JA014999

Müller-Wodarg, I. C. F., Aylward, A. D., & Lockwood, M. (1998). Effects of a mid-latitude solar eclipse on the thermosphere and ionosphere—A modelling study. *Geophysical Research Letters*, *25*, 3787–3790. https://doi.org/10.1029/1998GL900045

Nava, B., Coisson, P., & Radicella, S. M. (2008). A new version of the NeQuick ionosphere electron density model. *Journal of Atmospheric and Solar-Terrestrial Physics*, *70*(15), 1856–1862. https://doi.org/10.1016/j.jastp.2008.01.015

Salah, J. E., Oliver, W. L., Foster, J. C., & Holt, J. M. (1986). Observations of the May 30, 1984, annular solar eclipse at Millstone Hill. *Journal of Geophysical Research*, *91*, 1651–1660. https://doi.org/10.1029/JA091iA02p01651

Tsai, H. F., & Liu, J. Y. (1999). Ionospheric total electron content response to solar eclipses. *Journal of Geophysical Research*, *104*, 12,668, 12,657. https://doi.org/10.1029/1999JA900001

Zakharenkova, I., Astafyeva, E., & Cherniak, I. (2016). GPS and GLONASS observations of large-scale traveling ionospheric disturbances during the 2015 St. Patrick's Day storm. *Journal of Geophysical Research: Space Physics*, *121*, 12,138–12,156. https://doi.org/10.1002/2016JA023332

Zakharenkova, I., & Cherniak, I. (2015). How can GOCE and TerraSAR-X contribute to the topside ionosphere and plasmasphere research? *Space Weather*, *13*, 271–285. https://doi.org/10.1002/2015SW001162